

Transport across cell membranes is modulated by lipid order

Nicolas Färber, Jonas Reitler, Julian Schäfer, Christoph Westerhausen

Angaben zur Veröffentlichung / Publication details:

Färber, Nicolas, Jonas Reitler, Julian Schäfer, and Christoph Westerhausen. 2023. "Transport across cell membranes is modulated by lipid order." *Advanced Biology* 7 (6): 2200282. <https://doi.org/10.1002/adbi.202200282>.

Transport Across Cell Membranes is Modulated by Lipid Order

Nicolas Färber, Jonas Reitler, Julian Schäfer, and Christoph Westerhausen*

This study measures the uptake of various dyes into HeLa cells and determines simultaneously the degree of membrane lipid chain order on a single cell level by spectral analysis of the membrane-embedded dye Laurdan. First, this study finds that the mean generalized polarization (GP) value of single cells varies within a population in a range that is equivalent to a temperature variation of 9 K. This study exploits this natural variety of membrane order to examine the uptake as a function of GP at constant temperature. It is shown that transport across the cell membrane correlates with the membrane phase state. Specifically, higher membrane transport with increasing lipid chain order is observed. As a result, hypothermal-adapted cells with reduced lipid membrane order show less transport. Environmental factors influence transport as well. While increasing temperature reduces lipid order, it is found that locally high cell densities increase lipid order and in turn lead to increased dye uptake. To demonstrate the physiological relevance, membrane state and transport during an *in vitro* wound healing process are analyzed. While the uptake within a confluent cell layer is high, it decreases toward the center where the membrane lipid chain order is lowest.

account for all the membrane functions. The lipid molecules themselves are an interacting system whose physical properties such as bending rigidity and viscosity depend on its phase state given by the lipid order.^[1] Moreover, various examples indicate that lipids seem to foster particular cellular functions. For example the T-cell membrane lipid chain order increases during activation in the vicinity of activation sites and at the immunological synapse.^[2,3] The membrane phase state influences adhesion as membrane lipid chain order is increased at focal adhesion points.^[4] During virus budding highly ordered lipid regions are selectively incorporated into the influenza virus envelope.^[5] Even virus infectivity depends on the lipid order of its envelope and can be reduced by cholesterol depletion^[6] which is known to alter lipid order.^[7,8] Cell membrane phase state dependent transport is so far mainly discussed in the context of

1. Introduction

The lipid double layer of cell membranes is more than a mere barrier between cellular environments carrying proteins that

lipid rafts that affect vesicular transport.^[9,10] Lipid chain order transitions and temperature dependent cell membrane transport by passive diffusion however is pre-eminently object of cryobiology and sample cold storage.^[11–14] We want to focus on membrane transport as phase state dependent cellular function and were inspired by synthetically created lipid membrane model systems such as phospholipid vesicles and black lipid membranes which exhibit a permeability maximum at the phase transition between the gel and the fluid phase due to increased pore formation within the membrane at the phase transition.^[15,16] Such transitions have been measured so far calorimetrically and optically in biological membranes as well.^[14,17,18] For optical analysis one suitable membrane phase state probe is the fluorescent membrane-embedded dye Laurdan whose emission spectrum depends on the polarity and the relaxation dynamics of its environment.^[19,20] The emission maximum shift of Laurdan from 440 to 490 nm upon decreasing lipid order can be quantified by the generalized polarization (GP)^[21] which depends linearly on the lipid chain order.^[22] Here, we determined GP on a single cell level by fluorescence microscopy and the use of two different emission filters to detect the wavelengths around $\lambda = 440$ and 490 nm as shown in **Figure 1**. In this context a low GP value corresponds to a low degree of lipid order and therefore a rather fluid cell membrane whereas high GP values indicate a highly ordered cellular membrane. Due to the internalization of Laurdan and the staining of inner membranes that are not involved into membrane transport

N. Färber, C. Westerhausen
Experimental Physics I
Institute of Physics
University of Augsburg
Universitätsstraße 1, 86159 Augsburg, Germany
E-mail: christoph.westerhausen@gmail.com;
christoph.westerhausen@uni-a.de
N. Färber, J. Reitler, J. Schäfer, C. Westerhausen
Physiology
Institute of Theoretical Medicine
University of Augsburg
Universitätsstraße 2, 86159 Augsburg, Germany
C. Westerhausen
Center for NanoScience (CeNS)
Ludwig-Maximilians-Universität Munich
80799 Munich, Germany

 The ORCID identification number(s) for the author(s) of this article can be found under <https://doi.org/10.1002/adbi.202200282>.

© 2023 The Authors. Advanced Biology published by Wiley-VCH GmbH. This is an open access article under the terms of the Creative Commons Attribution-NonCommercial-NoDerivs License, which permits use and distribution in any medium, provided the original work is properly cited, the use is non-commercial and no modifications or adaptations are made.

DOI: 10.1002/adbi.202200282

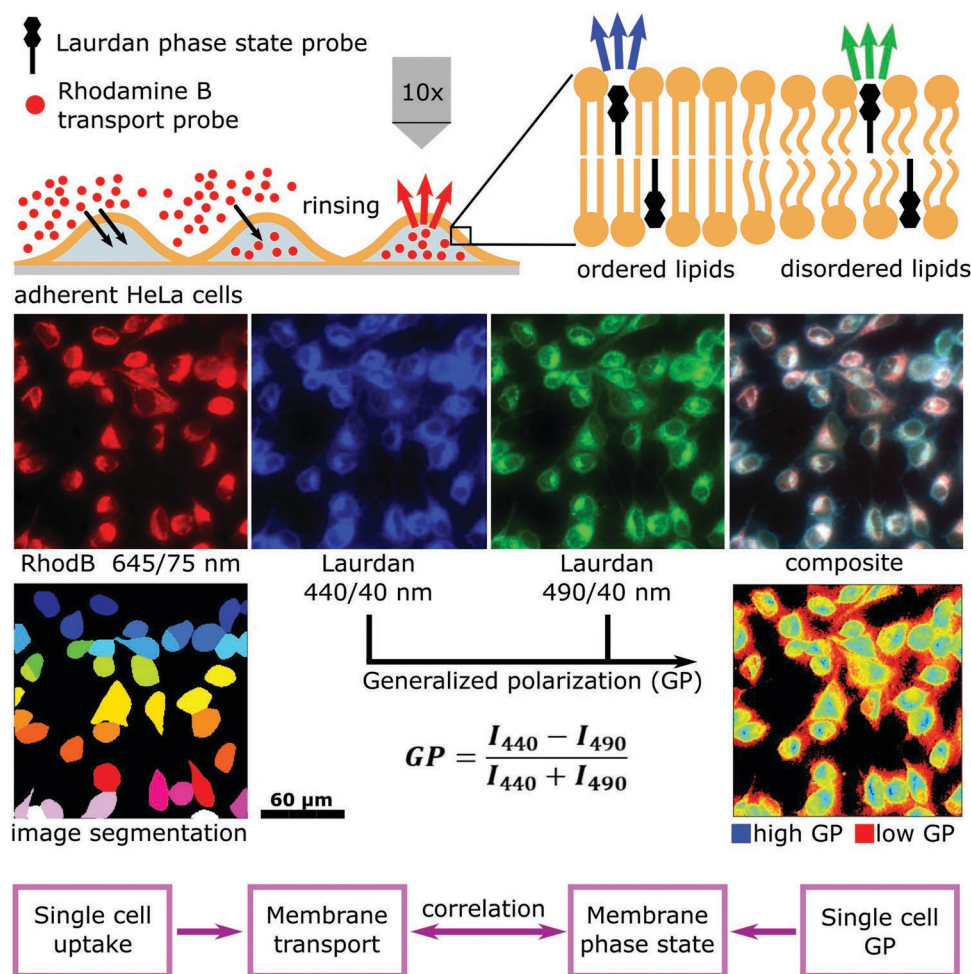


Figure 1. Experimental procedure and data analysis. The concept of simultaneous analysis of membrane phase state and membrane transport is visualized in the sketch above. The emission spectrum of the membrane-embedded dye Laurdan shifts from blue (440 nm) to greenish (490 nm) with increasing lipid disorder therefore indicating the membrane phase state while the fluorescence intensity of rhodamine B acts as a measure for the amount of dye molecules transported into the cell. The spectral changes of Laurdan are measured using of two different emission filters and quantified by the generalized polarization (GP). Image segmentation performed by a neural network allows for determination of single cell uptake and GP values. With these we answer the question whether cell membrane phase state and transport across the membrane are correlated.

processes we conducted a spatially resolved analysis using fluorescence microscopy that distinguishes between inner and outer membranes (Figure S4, Supporting Information). For simultaneous determination of cell membrane transport, we exposed adherent HeLa cells to rhodamine B and measured its fluorescence intensity after background reduction by rinsing in a third channel to quantify the dye uptake using fluorescence microscopy as indicated in Figure 1. We chose HeLa cells because of their easy handling and their wide spread among research groups. State of the art image segmentation using the python module cellpose of Stringer et al. enabled us to ascribe pixel GP and pixel rhodamine B intensity values to single cells and to calculate mean GP and mean rhodamine B intensities for each cell.^[23] By comparison of the quantities GP and rhodamine B uptake we answer the question whether membrane phase state and membrane transport are correlated. In a recent publication we analyzed the membrane phase state of Laurdan stained HeLa cell suspension over a wide temperature range and found a lipid chain order transition that extends over a temperature

range from $-40\text{ }^{\circ}\text{C}$ to $90\text{ }^{\circ}\text{C}$ which is shown in Figure 2a.^[8] If the permeability of cell membranes is highest at the phase transition as observed for synthetic lipid membranes, we expect increased rhodamine B transport due to passive diffusion for cell membranes with a GP value of zero corresponding to an equal amount of ordered and disordered lipid chains, meaning the phase transition.

The structure of this study is as follows. First, we examine the cell membrane permeability by Rhodamine B uptake in various GP ranges by varying the temperature. Second, the Rhodamine B uptake of HeLa cells that adapted lipid chain order to hypothermal culture temperature and have in consequence a lower GP value is compared to cells cultured at standard conditions. Third, we validate the Rhodamine B results by time resolved transport measurements using Hoechst 33342 as membrane transport probe. Ultimately, the membrane phase state and transport dependency on local cell density is analyzed and its physiological relevance is demonstrated in the context of wound healing.

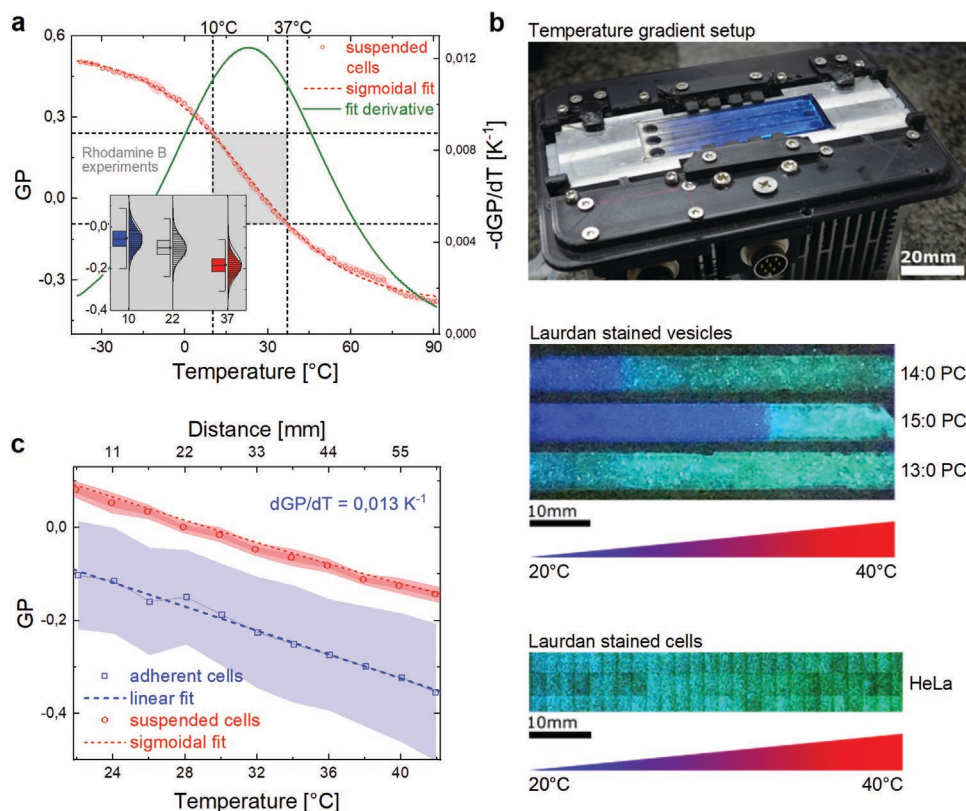


Figure 2. Temperature dependent phase state of adherent cells. a) The temperature dependent generalized polarization of suspended HeLa cells and its derivative with respect to temperature show that HeLa cell membranes undergo a phase transition that extends from -30°C to 90°C . The permeability measurements conducted in this study were carried out close to a physiological temperature regime (10°C , 22°C , and 37°C) that is located right in the center of the broad phase transition where temperature changes have the biggest impact on lipid chain order. b) Merged photography (room lighting and UV lamp) of an aluminum block that allows for temperature gradient exposure of cell overgrown glass slides via peltier cooling/heating on the backside. While vesicles consisting of pure phospholipids show sharp lipid order transitions indicated by the abrupt change of Laurdan emission color HeLa cells undergo a far less steep transition. c) The temperature dependent generalized polarization (GP) of the suspended cells shown in Figure 2a is plotted around a physiological temperature regime together with the GP of adherent cells. Both show a similar slope of 0.013 K^{-1} but a difference of absolute GP. In case of the suspended cells, symbols indicate the mean of three independent experiments in which one global phase state value per temperature point of a cell suspension was measured. The red bands show standard deviation and standard error. In case of the adherent cells, symbols represent the mean value of three independent experiments containing each 5000 cells per temperature interval. The blue colored band indicates the standard deviation. The standard error band is too narrow to be shown here.

2. Experimental Section

Fluorescence microscopy was performed on a Zeiss Axiovert 200 M epi-fluorescence microscope. The Laurdan (Sigma-Aldrich Chemie GmbH, Munich, Germany) fluorescence was analyzed with different filter sets using the same excitation wavelength of 350/50 nm but different emission filters: 440/20 and 490/20 nm. The latter was used for Hoechst 33342 (NucBlue, Sigma-Aldrich Chemie GmbH, Munich, Germany) measurements as well. For imaging of rhodamine B (Sigma-Aldrich Chemie GmbH) we used an excitation range of 585/30 and an 624/40 nm emission band-pass. The emission spectra of Laurdan, Hoechst 33 342 and Rhodamine B were recorded using an Ocean optics QEPro spectrometer.

Image analysis started with stitching of single images using the Fiji plugin of Preibisch et al.^[38] This was followed by image segmentation using the python package cellpose of Stringer et al.^[23] The image intensity data was further processed in a python script. Cell mean GP was calculated by summing up the GP values of each single cell pixel using the according pixels in

the 440 and 490 nm emission images followed by division by the number of cell pixels. The dye uptake intensity was determined in the same way as sum of pixel intensities normalized to the number of pixels. For the nearest neighbor analysis, the centroids of each cell were calculated as the center of mass. Surrounding cells were identified as neighbors if the Euclidean distance between the centers of mass was lower than $31\ \mu\text{m}$.

HeLa cells (ATCC CCL-2) were cultured in 25 cm^2 NuncTM cell culture flasks (ThermoFisher Scientific, MA, USA) at 37°C in saturated atmosphere in DMEM (Bio&SELL GmbH, Nürnberg, Germany) supplemented with 10% fetal bovine serum (FBS Superior) and 1% Pen/Strep (Biochrom GmbH, Berlin, Germany). For fluorescence microscopy cells were trypsinated with 1 ml of 0,05% trypsin/EDTA (Biochrom GmbH) and about 0.2 Mio. cells were transferred into a custom-made culture vessel with 5.5 cm^2 glass bottom and incubated for 24 h in culture medium. Prior to the uptake experiments cell membranes were stained in culture medium after addition of Laurdan dissolved in dimethyl sulfoxide (DMSO, 1 mg mL^{-1})

for 2 h at 37 °C. The final concentration of Laurdan and DMSO in the staining solution were 28×10^{-6} M and 141×10^{-3} M (11 mg L^{-1}).

For Rhodamine B uptake measurements, the temperature of the Laurdan stained cells was adjusted to either $T = 10$ °C, $T = 22$ °C or $T = 37$ °C with a custom-made microscope insert. After equilibration monitored with a PT100 temperature sensor tempered culture medium containing Rhodamine B was added to the culture vessel yielding a dye concentration of 1×10^{-3} M. After 10 min of Rhodamine B exposure the cells were thoroughly rinsed with tempered PBS buffer for at least five times. 3-channel imaging (Laurdan at 440 nm, Laurdan at 490 nm and rhodamine at 624 nm) was carried out under PBS buffer at the according temperature.

Hoechst 33342 uptake measurements were carried out at $T = 22$ °C. After Laurdan staining cells were directly imaged with two channels (Laurdan 440 and 490 nm). Afterwards tempered culture medium containing Hoechst 33342 was added to the culture vessel yielding a dye concentration of 8×10^{-6} M. Immediately after addition the increasing Hoechst 33342 fluorescence was recorded by consecutive 1-channel (Laurdan and Hoechst 33342 at 490 nm) scans. During intensity data processing the Hoechst 33342 intensity was corrected for Laurdan intensity.

For wound healing analysis we placed 2-well silicone culture inserts (Ibidi GmbH, Gräfelfing, Germany) with a growth area of 0.22 cm^2 per well and a cell free gap of around $500 \mu\text{m}$ onto glass slides. After filling each well with about 50 000 cells the slides were incubated for 24 h followed by removal of the silicone insert. Laurdan staining was carried out after $t = 6, 12,$ and 24 h at $T = 37$ °C as described above. Afterwards the cells were exposed to 1×10^{-3} M Rhodamine B in culture medium for 10 min at 22 °C followed by rinsing with phosphate buffered saline (PBS) for at least five times. Finally, three channels were imaged (Laurdan at 440 nm, Laurdan at 490 nm, and Rhodamine B at 624 nm).

2.1. Data Representation

All data shown originates from at least three independently conducted experiments. In the case of GP-histograms we used throughout a bin size of 0.01 and summed up the counts of three independent datasets each contributing the same number of cells as can be seen in the raw data plot in Figure S3 (Supporting Information). For comparison these histograms were normalized to zero and one as shown in Figures 3 and 4. The according intensity datasets were reduced by sorting the GP and rhodamine B intensity tuples of all three experiments ascending according to GP and calculating the mean, standard deviation, and standard error for a constant number of consecutive values. For this number we chose the square root of the number of all datapoints.

2.2. Statistics

Two tailed *t*-tests for 5% statistical significance between two values were performed with four degrees of freedom corresponding to six independently measured samples. In

addition we calculated *t*-values with a higher degree of freedom using an effective sample size obtained by ICC analysis based on Liljequist et al.^[39]

3. Results and Discussion

In this study, we conducted membrane transport measurements of adherent HeLa cells around a physiological temperature regime from 10 °C to 37 °C which is located right in the middle of the lipid chain order transition of a HeLa cell suspension shown in Figure 2a. In order to examine whether the transition regime of adherent cells differs from the one of suspended cells, we determined the phase state of adherent HeLa cells in a temperature gradient setup that is shown in Figure 2b. The difference between phase transitions of biological and synthetic membranes can be clearly seen in the fluorescence emission color of Laurdan pictured below the gradient setup. While the phospholipid vesicles display a steep transition from greenish to blue indicating a sudden change of lipid chain order with respect to temperature the transition of HeLa cell membranes is much broader and continuous. The comparison of the GP change per temperature of suspended and adherent cells shown in Figure 2c yields that except for the absolute GP value the steepness of the transition is in both cases similar with a slope of $\frac{dGP}{dT} = 0.013 \text{ K}^{-1}$ which allows for conversion of GP changes to equivalent temperature changes. While the measurement of suspended cells yields only a mean value of the whole cell ensemble, the analysis of adherent cells by fluorescence microscopy allows for single cell uptake and phase state determination. By this we were able to measure the broadness of the GP distribution shown in Figure 2c as the standard deviation of the single cell GP values colored in blue, whereas the red colored band indicates the standard deviation between the three independent measurements of suspended cells. This natural variance in membrane lipid chain order enabled us to measure rhodamine B uptake as measure for membrane transport as function of membrane phase state quantified by GP.

We have chosen different dyes to examine the transport process into HeLa cells due to experimental constrictions when measuring GP and dye uptake intensity within one experiment. While the Rhodamine B emission spectrum does not interfere with the Laurdan emission allowing for simultaneous imaging of both dyes, it is still necessary to minimize background fluorescence by rinsing. Moreover, for the compensation of its temperature dependent quantum yield we recorded a calibration curve shown in Figure S1a (Supporting Information). Furthermore, we excluded that Rhodamine B has a significant influence on the cell membrane phase state or the Laurdan emission spectrum because of channel cross-talk or Förster resonance energy transfer (FRET). Indeed, we observed that Rhodamine B exposure increases lipid order in average by 0.04 as shown in Figure S1b (Supporting Information) which is well below the effects that will be discussed in the following passage. To eliminate the influence of the permeability probe on the membrane phase state or the Laurdan emission properties we have conducted experiments in which we analyzed the phase state of cells prior to the permeability measurements.

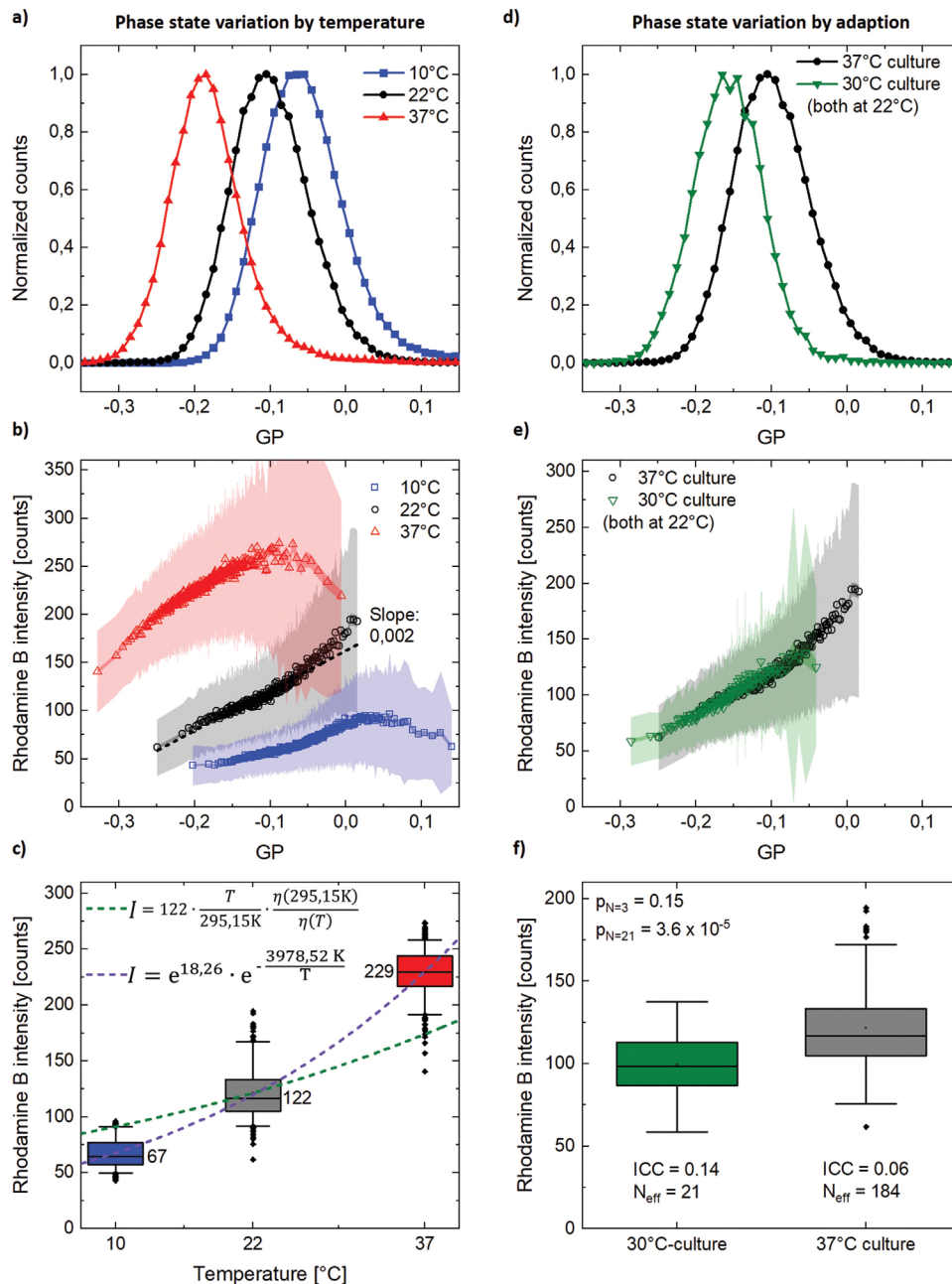


Figure 3. Phase state dependent rhodamine B uptake. a) Distribution of single cell generalized polarization (GP) values within a population at three different temperatures. With increasing temperature the distributions shift toward lower GP values meaning less lipid chain order. Using the GP slope obtained in Figure 2b of $dGP/dT = 0.013 \text{ K}^{-1}$ the width of the histograms can be associated with a temperature interval of 9 K width. b) Rhodamine B intensity within cells as measure for cell membrane transport as function of GP measuring lipid chain order recorded at three different temperatures. High temperatures allow for investigation of low GP values meaning low lipid chain order and vice versa. The symbols represent the mean value of a GP interval of three independent experiments. The two colored bands indicate standard deviation and standard error. The temperature dependence of Rhodamine B intensity was corrected. c) Box plot of the Rhodamine B intensity plotted in (b). The green dotted line indicates the uptake behavior relative to $T = 22^\circ\text{C}$ as a function of temperature and temperature dependent viscosity regarding only the diffusion coefficient of water. The data is better approximated by an Arrhenius model which is indicated as purple dashed graph. d) Histograms of GP values of two differently cultured HeLa cell populations measured at the same temperature of 22°C . The cells that were cultured at 30°C for 1 year exhibit less lipid chain order compensating the temperature induced increased lipid chain order during growth. e) Comparison of rhodamine B transport measurements as a function of GP of two differently cultured cell populations at the same temperature. Since the hypothermal adapted cells cover a lower GP range, it is possible to measure transport phenomena as function of phase state without temperature effects. f) Box plot of the Rhodamine B intensity of cold adapted and reference HeLa cells. Since the adapted population covers a lower GP range in (e) that is associated with lower dye uptake the mean rhodamine B intensity is lower than for the reference cells. The first p -value was calculated using a sample size of $N = 3$ corresponding to three independently conducted experiments. For the second calculation we used the effective sample size of 21 obtained by ICC analysis.

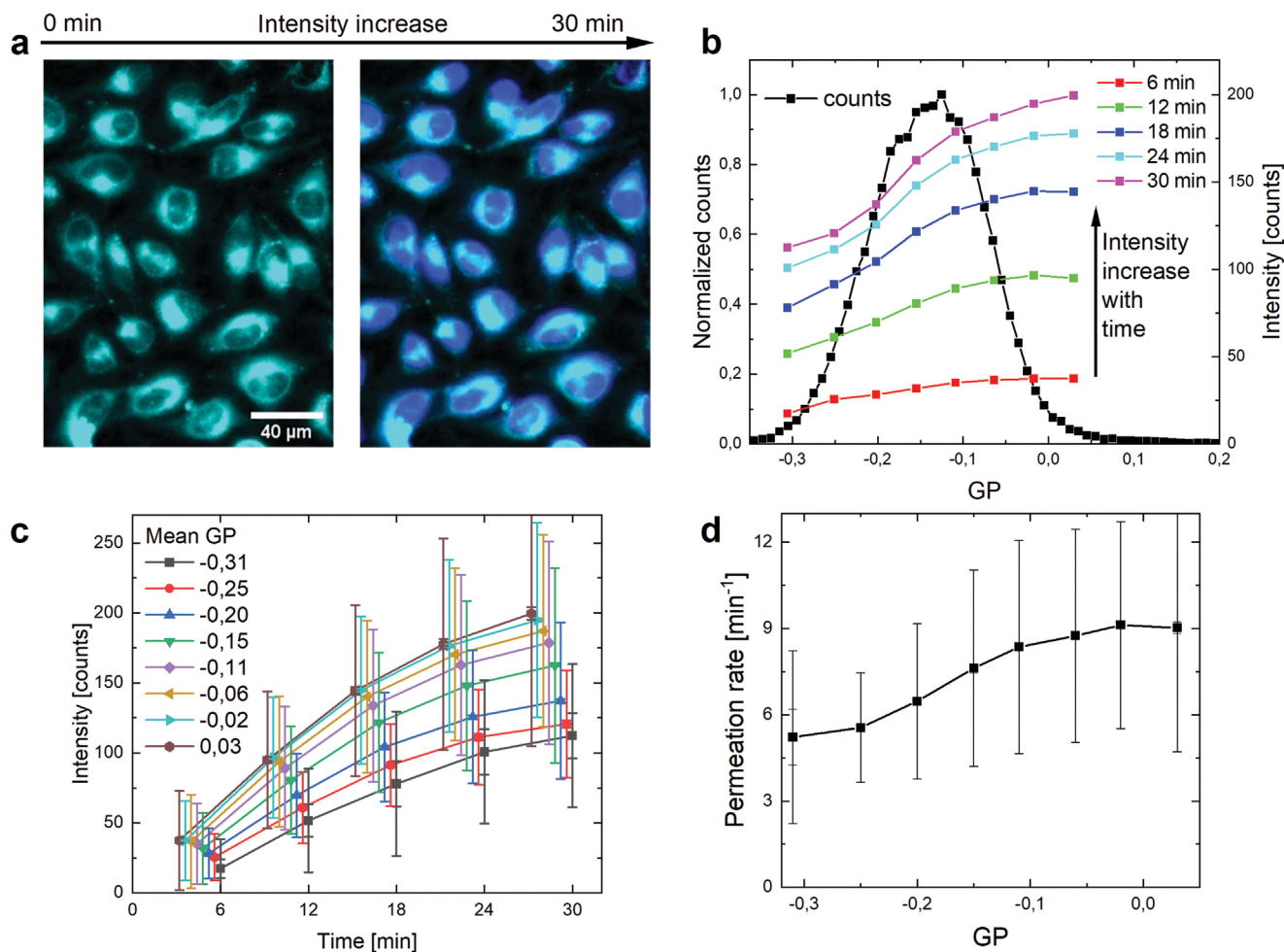


Figure 4. Phase state dependent Hoechst 33342 uptake. a) Fluorescence micrograph of Laurdan (cyan) stained HeLa cell membranes prior and after addition of Hoechst 33342 (blue). b) Generalized polarization (GP) distribution as the normalized sum of three independent experiments and time course of GP dependent Hoechst 33342 mean intensity. c) Hoechst 33342 mean intensity as function of time for different mean GP values. Error bars indicate standard deviation and standard error. Each graph is shifted by 0.04 min for better visibility. d) Permeation rate as function of GP obtained by fitting of the data set presented in (c). Error bars indicate standard deviation and standard error.

For this we analyzed the uptake of Hoechst 33342 that only fluoresces after transport into the cells making it possible to record kinetics without rinsing steps. In this case the Laurdan stained membrane was imaged before Hoechst 33342 addition to avoid any interference due to FRET or fluorescence channel cross-talk.

3.1. Temperature and Phase State Dependent Rhodamine B Uptake

The first observation of the single cell Laurdan phase state analysis is that the GP value averaged over one cell varies within a cell population at constant temperature in a GP range of about $\text{FWHM}_{\text{GP}} = 0.12$ (Figure 3a). Considering the GP dependency on temperature of 0.013 K^{-1} (Figure 2b) this can be associated with a change in lipid chain order induced by a temperature variation of $\text{FWHM}_T = 9 \text{ K}$. Such GP variations were reported by Parasassi et al. for other cell types as well.^[24] The natural variety of the cell membrane phase state between single cells

enabled us to examine the uptake of fluorescent dyes as a function of GP without the need for manipulating the membranes in any way. As only the outer cell membrane is involved in the transport process and Laurdan stains inner membranes to some extent as well we analyzed the outer and inner cell regions separately in Figure S4 (Supporting Information). We found that the uptake of rhodamine B correlates much stronger with the lipid order of the outer membrane regions as compared to the GP value in the cell center. However, we continue for simplicity with the average GP over the whole cell membrane as it is dominated by the outer membrane GP values as can be seen in Figure S4 (Supporting Information).

The result of this analysis recorded at a temperature of $22 \text{ }^\circ\text{C}$ is shown in Figure 3b. We observed a monotonic increase of Rhodamine B uptake into the cells with increasing lipid chain order measured by GP. The maximum uptake is located at a GP value around zero but only few datapoints could be collected in this region as the GP distribution does not extend into the range above $\text{GP} = 0$ (Figure 3a) at $T = 22 \text{ }^\circ\text{C}$. To verify that there is indeed a GP dependent Rhodamine B uptake and not

only a GP dependency on Rhodamine B due to FRET we use a linear fit to approximate the data of the 22 °C experiment in Figure 3b and calculate that rhodamine B would have to change GP by 2×10^{-3} per count intensity. The comparison of the mean GP values of two Laurdan stained cell populations, one after Rhodamine B exposure emitting a mean fluorescence of 122 counts and one reference, reveals a GP shift of 0.04 (Figure S1b, Supporting Information) meaning that Rhodamine B shifts the cell membrane GP in average only by 3×10^{-4} per count. Thus, the effect is one order of magnitude lower. To exclude GP dependencies on cell size and in consequence on the rhodamine B uptake we plotted GP as a function of the cell membrane area in Figure S2a (Supporting Information). We found no pronounced size dependency and obtained a Pearson-correlation coefficient of $r = 0.03$. Furthermore, we analyzed the phase state dependent Rhodamine B uptake for different cell sizes and observed the same trend for every cell size as shown in Figure S2b (Supporting Information).

A GP of zero implies that Laurdan emits just as much intensity at 440 nm as at 490 nm meaning that approximately an equal numbers of lipid chains are in the ordered and disordered state. In the context of lipid membrane phase state this indicates the phase transition regime. At this point synthetic lipid membranes exhibit the highest permeability as it was shown by Blicher et al. who measured the permeation rate of DPPC/DPPG vesicles as a function of temperature.^[16] To examine the applicability of this concept to the far more complex system of cell membranes we studied the GP dependent Rhodamine B uptake at lower temperatures where lipid chain order is increased and therefore the GP distribution extends to higher values. The result is shown in Figure 3b. The increasing emission intensity of rhodamine B with decreasing temperature was corrected using the calibration curve in Figure S1a (Supporting Information). The GP histogram recorded at 10 °C is clearly shifted toward higher values compared to the 22 °C sample enabling us to study the membrane transport beyond a GP value of zero. Indeed, the uptake of rhodamine B shows a maximum around $GP = 0.025$ and decreases again with increasing lipid chain order. Therefore, the results of the $T = 10$ °C and 22 °C measurements could be described by a model of phase state dependent passive diffusion through the cell membrane lipid bilayer.

To cover the most relevant phase state regime we conducted further experiments at a temperature of $T = 37$ °C. Due to temperature induced reduced lipid chain order the GP distribution in Figure 3a is shifted toward lower values. In line with the passive diffusion model an increasing dye uptake from a GP of $GP = -0.3$ to -0.1 can be seen in Figure 3b. This trend is followed by decreased uptake toward zero GP. Based on this outcome we conclude that in addition to passive diffusion active processes must be involved in the transport mechanism of Rhodamine B across the HeLa cell membrane as well. High magnification fluorescence micrographs shown in Figure S1c (Supporting Information) support this assumption as they show on the one hand uniform Rhodamine B intensity distributed over the whole cytosol, but on the other hand vesicular structures exhibiting high Rhodamine b intensity. The latter could indicate endocytosis-like uptake as discussed in the literature in the context of lipid rafts.^[9,10] To estimate the portion

of vesicular Rhodamine B uptake we compared the mean and median intensities within the cells as the median is less sensitive to few small regions of high intensity (Figure S1d, Supporting Information). As the comparison yields an intensity difference of only about 2% we conclude that passive diffusion is the main mechanism causing the phase state dependent Rhodamine B uptake shown here. This is in agreement with studies proposing passive diffusion of Rhodamine B through lipid bilayers by translocation.^[40]

The absolute values of Rhodamine B intensity in Figure 3b increase with higher temperature which implies that the uptake is not only temperature dependent due to membrane properties. This effect can be seen in the intensity box plot of Figure 3c even clearer where the uptake of the whole cell population is analyzed GP independently. We assume that the diffusion of Rhodamine B itself through the extra and intracellular environment depends on temperature as well. In general, the diffusion coefficient of fluids is directly proportional to temperature and inversely proportional to viscosity which is temperature dependent as well. The result of this dependency applied to the 22 °C uptake intensity as reference value is shown in Figure 3c as green dashed line. While it describes our observations of increasing dye uptake with increasing temperature qualitatively well it still does not match the absolute values perfectly. Therefore, a model of totally unhindered Rhodamine B diffusion seems to be unlikely. Assuming that an activation energy is necessary to overcome the cell membrane leads to an Arrhenius ansatz as often used for membrane permeability determination.^[25,26] Figure S2c (Supporting Information) shows the Arrhenius plot of the mean rhodamine B intensity of the whole cell populations measured at $T = 10$ °C, 22 °C, and 37 °C. The parameters obtained by a linear fit were incorporated in the Arrhenius equation and plotted in Figure 3c. As the permeability data is well approximated by the Arrhenius equation we calculated the activation energies for three different GP intervals again by linear fitting of the Arrhenius plots in Figure S2d (Supporting Information) and obtained values ranging from 15 to 20 kJ mol^{-1} as shown in Figure S2e (Supporting Information).

In summary, we have shown for different temperatures that the transport of Rhodamine B correlates with the membrane phase state of HeLa cells. More precisely, the uptake increases over a wide GP range with increasing lipid chain order. At $T = 10$ °C and 37 °C we observed in addition local maxima that could be ascribed to passive diffusion or active transport mechanisms. A temperature increase affects this process in a way that it increases diffusion on one hand but decreases lipid chain order on the other hand. In turn, the latter inhibits transport to a certain degree.

3.2. Phase State Dependent Rhodamine B Uptake into Hypothermal Adapted Cells

Based on the results discussed above environmental changes that reduce lipid order should reduce Rhodamine B uptake as well. In the case of increasing temperature this effect is overruled by the increased dye diffusion. Earlier, we have shown that HeLa cells cultured at lower temperatures (30 °C) adapt

their membrane phase state by decreasing lipid chain order.^[8] Similar temperature adaption effects were observed in *E. coli* membranes, paramecium multimicronucleatum, and giant plasma membrane vesicles of zebra fish.^[17,18,27] A comparison of hypothermal adapted cells with their 37 °C cultured analogues enabled us to study two cell populations with different phase states at the same temperature. The effect of adaption can be seen in Figure 3d where the GP histogram of the cells cultured at 30 °C is shifted toward lower GP values meaning decreased lipid chain order. Furthermore, the distribution broadness decreases by 10% because of adaption which could indicate that the subpopulation of cells with high GP values is reduced stronger than the subpopulation with lower GP values in addition to a shift of the whole population. The Rhodamine B uptake shown in Figure 3e follows the same GP dependency as discussed for the 37 °C culture. The Rhodamine B uptake increases toward higher GP values showing no local maximum as observed for cells examined at $T = 10$ °C or 37 °C. The absolute Rhodamine B intensities match very well in the overlap region. Thus, the only difference between both samples is that in case of the adapted cells more cells are located at lower GP values corresponding to lower Rhodamine B uptake. This effect is reflected in the box plot of Figure 3f that shows the uptake of the whole cell populations without taking GP values into account. Because of the correlation of membrane phase state and membrane transport the HeLa cell population with lower lipid chain order shows less dye uptake.

3.3. Phase State Dependent Hoechst 33342 Transport Kinetics

To study the phase state dependent membrane transport time resolved and to exclude any interference of the permeability probe with the phase state probe we measured the uptake of Hoechst 33342 after the Laurdan phase state analysis. The nucleus staining dye Hoechst 33342 was used as membrane transport probe by Lalande et al. before and facilitates the measurement procedure as no rinsing steps are necessary because it only fluoresces after intercalation into DNA.^[28] As shown in Figure 4a the Laurdan stained cell membranes were imaged prior to Hoechst 33342 addition allowing for analysis of the uncompromised membrane and avoiding channel cross-talk. The Laurdan imaging recorded at $T = 22$ °C yields as before a GP distribution that is shown in Figure 4b. Directly after the phase state analysis Hoechst 33342 was added to the adherent cells and the increasing fluorescence intensity of the nucleus was imaged subsequently every 6 min. The GP dependent uptake measured by the fluorescence intensity is plotted in Figure 4b as well. The fluorescence increase is strongest at the beginning and saturates after 30 min. In addition, the uptake of cells with higher GP value is faster as compared to cells with low GP. To quantify this observation, we binned datapoints of equal GP and plotted their mean intensity as function of time shown in Figure 4c. As a result of a linear approximation of the beginning intensity increase, we obtained different permeation rates for cells of different GP values. By this we characterize membrane transport measured by the permeation rate as a function of phase state measured by GP as can be seen in Figure 4d. With increasing GP meaning increasing lipid

chain order the time constant measuring the permeation rate is increasing as well. Therefore, the correlation of membrane phase state and membrane transport in HeLa cells holds not only for Rhodamine B but for Hoechst 33342 as well and is not an artefact of the interference of the phase state probe and the membrane probe. As the DNA content as binding site of Hoechst 33342 may depend on the nucleus size we examined the GP dependence on the cell nucleus size in Figure S2f (Supporting Information). We could not identify a pronounced correlation between these quantities and obtained a Pearson correlation coefficient of $r = 0.01$.

3.4. Cell Density Dependent Membrane Phase State and Transport

Based on our findings, that permeability and lipid chain order are correlated, the question arises whether environmental changes that influence the cell membrane phase state would have impact on the membrane transport. To encounter this question, we first focused on a parameter that varied naturally within our samples: the local cell density. In our study to lipid phase transitions in cell membranes we found that morphological changes such as the transition from adherent to suspended during trypsinization were accompanied by changes in lipid order measured by GP.^[8] Therefore, we expected cell deformation induced by spatial confinement of neighbored cells should affect GP as well. This assumption indeed holds as can be seen in Figure 5a. The data were generated by analyzing the local environment of single cells. We defined cells with a distance of less than 31 μm between their centers of mass as neighboring cells. Then, we determined for each cell the number of neighbors as measure for local cell density (Figure 5b) and analyzed the membrane phase state by determining GP. The result for cells exclusively stained with Laurdan at $T = 22$ °C is shown in Figure 5a. The mean GP value increases from $\text{GP} = -0.17$ for cells without near neighbors up to $\text{GP} = -0.03$ for cells with seven neighbors, meaning that spatially more confined cells exhibit more lipid order than cells without surrounding cells. This is in agreement with findings of Steinkühler et al. who measured increased lipid order in giant plasma membrane vesicles of cells cultured at different cell densities.^[1] These changes in lipid order are likely to arise from alterations of the membrane lipid composition induced by the local cell environment.^[29,30] The observations that high lipid order is accompanied by high membrane transport (Figures 3 and 4) and that high cell densities induce high GP values suggest that high cell densities could lead to increased membrane transport.

To examine how cell density affects the membrane transport properties we executed the nearest neighbor analysis on Laurdan stained cells after Rhodamine B exposure at $T = 22$ °C yielding not only neighbor dependent phase state but dye uptake as well. In Figure 5c, the phase state analysis reveals that the mean GP of single cells after Rhodamine B exposure increases again monotonically from $\text{GP} = -0.11$ for zero neighbors up to $\text{GP} = -0.04$ for cells surrounded by seven other cells. The slightly elevated GP values are probably a result of the phase state influence of Rhodamine B itself. But the remarkable finding is that the membrane transport, measured by

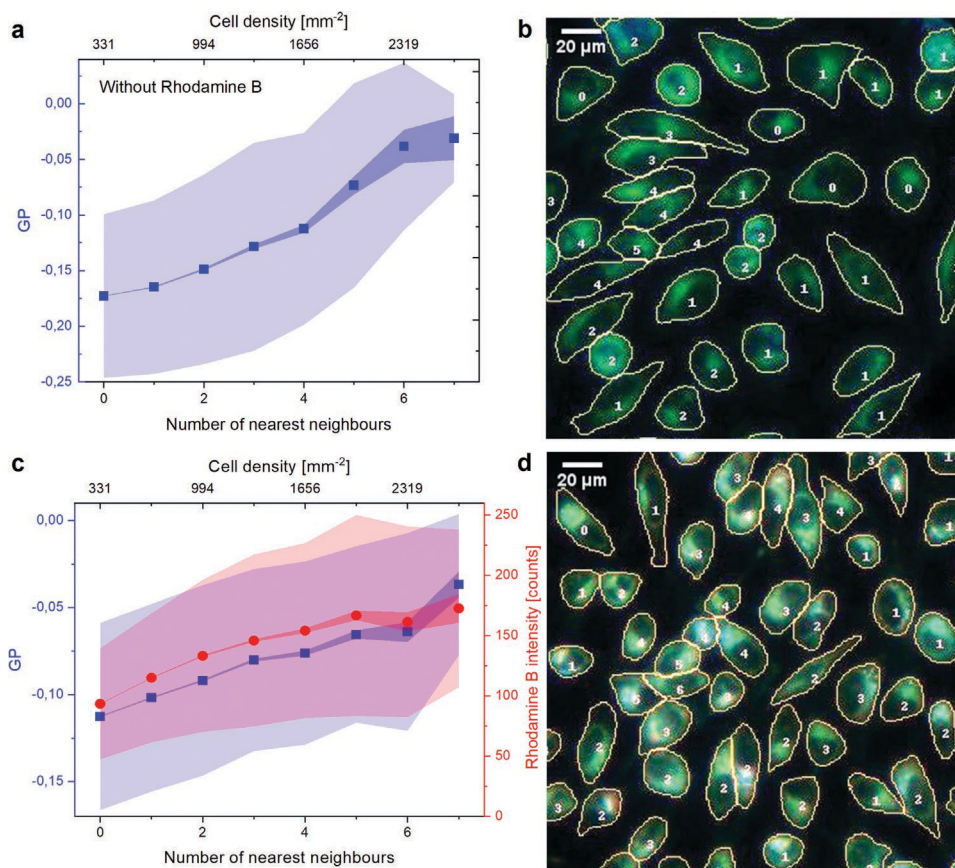


Figure 5. Cell membrane phase state and transport dependency on cell density. a) Mean cell generalized polarization (GP) as a function of the local cell density without Rhodamine B determined by the number of nearest neighbors (center of mass within a radius of $31\ \mu\text{m}$). The colored bands represent standard deviation and standard error. b) Fluorescence microscopy 2-channel image of HeLa cells stained with Laurdan and segmentation outlines labeled with the number of nearest neighbors. c) Mean cell GP and mean Rhodamine B intensity as a function of the number of cell neighbors. Lipid chain order increases with the number of neighbors causing the rhodamine B transport to increase as well. d) Fluorescence microscopy 3-channel image of HeLa cells stained with Laurdan and Rhodamine B.

Rhodamine B uptake, increases monotonically with increasing number of cell neighbors, too. This observation also can be detected by eye in Figure 5d and agrees with our results obtained by analyzing the phase state dependent transport of Rhodamine B and Hoechst 33342 at $T = 22\ ^\circ\text{C}$, where we observed the same GP dependent monotonic increase of dye uptake in HeLa cells. Therefore, we conclude that due to the correlation of cell membrane phase state and membrane transport capabilities, environmental factors that influence the cell membrane phase state have a direct impact on cell membrane transport.

To demonstrate the physiological relevance of this concept, we applied it to a wound healing assay. Here, a steep cell density gradient is present between a confluent cell layer and a cell free gap, simulating an artificial wound. Experimentally this was achieved by removal of a silicone culture insert and imaging of the wound after staining with Laurdan and Rhodamine B. To monitor the process of healing we analyzed three different timepoints after removal of the culture insert: $t = 6, 12,$ and $24\ \text{h}$. The GP value 6 h after wound creation is displayed in Figure 6a as a function of horizontal position within the wound assay shown on the right side as a fluorescence micrograph. In the high cell density regions of the confluent cell layer left and

right to the cell free area the mean GP reaches values of up to $\text{GP} = 0.04$ meaning high lipid chain order, while the mean GP within the artificial wound is as low as $\text{GP} = -0.06$ meaning low lipid chain order. As predicted from our findings on the correlation of GP and permeability above, the Rhodamine B uptake follows the spatial GP dependency in these regions. During this time interval, the cells migrated about $100\ \mu\text{m}$ toward the cell free gap during wound healing. In this region around the initial wound border the Rhodamine B uptake decreases with decreasing cell density toward a minimum of 140 counts. Interestingly, cells with low plasma membrane bending rigidity corresponding to decreased lipid order, as reported by Steinkühler et al.^[1], show increased migration.^[31] Therefore, it is possible that the reduced lipid chain order of cells located at the wound border with a low number of neighbors contributes to the initiation of cell migration and thus the wound healing process. After 12 h as shown in Figure 6b the lipid order and membrane transport in the confluent region is even more increased as compared to the 6 h measurement. This might be due to even higher cell density because of further cell proliferation. At this time point cells migrated about $200\ \mu\text{m}$ into the cell free gap. The decrease of lipid order and Rhodamine B uptake in the

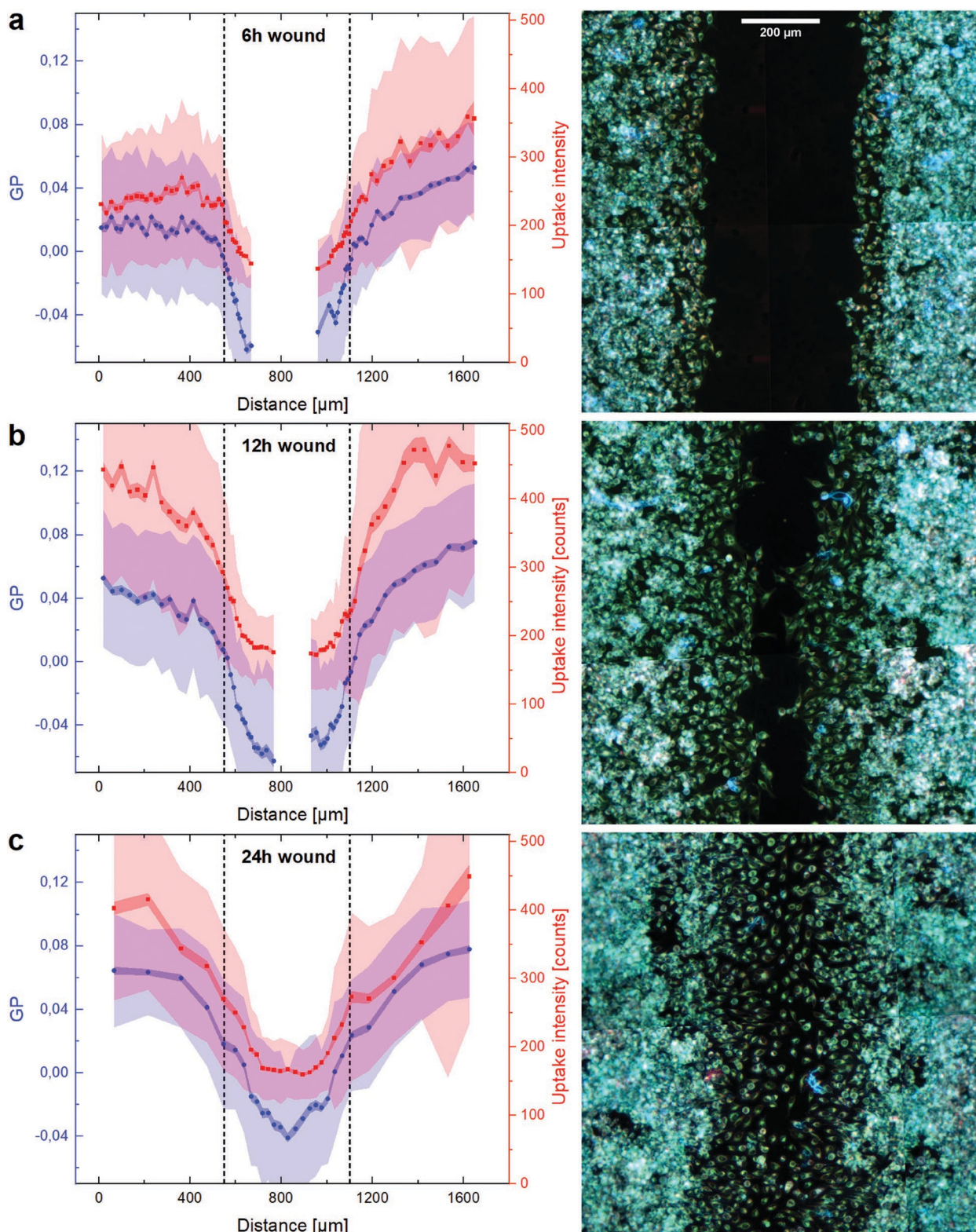


Figure 6. Phase state and transport analysis in the context of a wound healing process. a) Mean generalized polarization (GP) and Rhodamine B intensity as function of horizontal position within the wound healing assay pictured on the right side. The image was recorded and analyzed 6 h after wound creation by removal of a silicon culture insert. The initial borders of the wound are indicated in the graph on the left as dotted vertical lines. The colored bands indicate standard deviation and standard errors of the according quantities. As observed in the nearest neighbor analysis shown in Figure 5c GP and Rhodamine B intensity decrease toward the wound center corresponding to lower cell density. b) Wound phase state analysis 12 h after culture insert removal. The wound closure is more advanced compared to the data of Figure 6a. c) After 24 h HeLa cells migrated into the wound center, but the cell density is still much lower compared to the confluent regions to the left and to the right. As a result, lipid chain order and Rhodamine B uptake are still decreased in the wound center.

region from the initial wound border toward the wound center is less steep as compared to the 6 h sample as the gradient from maximal cell density in the confluent region to zero density in the cell free gap extends over a larger distance of 200 μm . Even though the wound is closed after 24 h which can be seen on the micrograph on the right side of Figure 6c there is still a large difference in cell density in the image center as compared to the border. This is reflected in the spatially dependent GP and Rhodamine B uptake in Figure 6c on the left side as well where the lipid order and dye uptake are still minimal in the wound center. But compared to the 6 and 12 h measurements the minimum GP values are slightly enhanced as cell density starts to increase even in the wound center.

In the context of wound healing, we have shown that high cell densities induce ordering of the lipid chains in HeLa cells which in turn leads to an increase of transport across the membrane. As a maybe counterintuitive result cells that do not have any neighbors and which are therefore much more exposed to any environmental influences show much less dye uptake than cells within a dense cell layer.

4. Conclusion

In summary we have shown for HeLa cells that there is a direct proportionality of cell membrane lipid chain order to the transport across the cell membrane in a wide range of GP. As consequence, single cells with a disordered membrane are less likely to take up molecules from the environment compared to cells with a higher lipid chain order at the same temperature. Even though we only conducted experiments with HeLa cells we think that the dependence of membrane transport on lipid order could be a universal concept that holds for other cell types as well.

Moreover, we demonstrated that environmental factors that influence the physical cell membrane state, such as cell density, directly affect membrane transport. This finding allows for prediction of cell membrane transport properties under other environmental influences if their effect on the lipid phase state is known. These influences changing the lipid order of biological membranes of various cell types, for example, can be changes in pH, solvent exposure, anesthesia, and cholesterol content modulations, as we have shown earlier.^[8] Others have shown that lipid chain order measured by GP is altered by salt concentration or shear flow exposure.^[32,33] In the context of nerve pulse propagation dynamic transitions from an unordered to an ordered lipid membrane state are discussed as signal carrier.^[34] Our findings would further support this idea, as it explains the increased ion permeability during the propagation of an action potential.^[35–37] It would be very exciting to further elucidate the correlation of the cell membrane state and other cellular functions, as, e.g., enzyme activity, migration, adhesion, or reversible deformation.

Supporting Information

Supporting Information is available from the Wiley Online Library or from the author.

Acknowledgements

The authors thank Matthias Schneider, Simon Fabiunke, and Achim Wixforth for fruitful discussions. The authors thank the Center for Nanoscience (CeNS) and the Augsburg Centre for Innovative Technologies (ACIT) for funding. C.W. would like to acknowledge funding for the project “Physical and functional interaction mechanisms at cell membranes and vessel walls” by the University of Augsburg. N.F. would like to thank the Joachim Herz foundation.

Open access funding enabled and organized by Projekt DEAL.

Conflict of Interest

The authors declare no conflict of interest.

Author Contributions

N.F. and C.W. designed research. N.F., J.S., J.R., and C.W. performed research. N.F., J.S., and J.R. analyzed data and implemented experimental tools. N.F. and C.W. wrote the paper.

Data Availability Statement

The data that support the findings of this study are available from the corresponding author upon reasonable request.

Keywords

generalized polarization, Laurdan, lipid membrane state, membrane permeability, order disorder phase transitions, wound healing

Received: October 20, 2022
Revised: December 13, 2022
Published online: January 18, 2023

- [1] J. Steinkühler, E. Sezgin, I. Urbančič, C. Eggeling, R. Dimova, *Commun. Biol.* **2019**, *2*, 337.
- [2] K. Gaus, E. Chklovskaya, B. Fazekas De St Groth, W. Jessup, T. Harder, *J. Cell Biol.* **2005**, *171*, 121.
- [3] D. M. Owen, S. Oddos, S. Kumar, D. M. Davis, M. A. A. Neil, P. M. W. French, M. L. Dustin, A. I. Magee, M. Cebecauer, *Mol. Membr. Biol.* **2010**, *27*, 178.
- [4] K. Gaus, S. L. Lay, N. Balasubramanian, M. A. Schwartz, *J. Cell Biol.* **2006**, *174*, 725.
- [5] P. Scheiffele, A. Rietveld, T. Wilk, K. Simons, *J. Biol. Chem.* **1999**, *274*, 2038.
- [6] D. R. M. Graham, E. Chertova, J. M. Hilburn, L. O. Arthur, J. E. K. Hildreth, *J. Virol.* **2003**, *77*, 8237.
- [7] D. B. Iaea, F. R. Maxfield, *PLoS One* **2017**, *12*, 6.
- [8] N. Färber, C. Westerhausen, *Biochim. Biophys. Acta, Biomembr.* **2022**, *1864*, 183794.
- [9] M. F. Hanzal-Bayer, J. F. Hancock, *FEBS Lett.* **2007**, *581*, 2098.
- [10] E. Ikonen, *Curr. Opin. Cell Biol.* **2001**, *13*, 470.
- [11] W. F. Wolkers, H. Oldenhof, F. Tang, J. Han, J. Bigalk, H. Sieme, *Langmuir* **2019**, *35*, 7520.
- [12] M. Akhoondi, H. Oldenhof, C. Stoll, H. Sieme, W. F. Wolkers, *Biochim. Biophys. Acta* **2011**, *1808*, 642.
- [13] W. F. Wolkers, L. M. Crowe, N. M. Tsvetkova, F. Tablin, J. H. Crowe, *Mol. Membr. Biol.* **2002**, *19*, 59.

- [14] J. H. Crowe, F. A. Hoekstra, L. M. Crowe, T. J. Anchordoguy, E. Drobnis, *Cryobiology* **1989**, 26, 76.
- [15] L. Cruzeiro-Hansson, O. G. Mouritsen, *Biochim. Biophys. Acta, Biomembr.* **1988**, 944, 63.
- [16] A. Blicher, K. Wodzinska, M. Fidorra, M. Winterhalter, T. Heimbürg, *Biophys. J.* **2009**, 96, 4581.
- [17] T. Toyoda, Y. Hiramatsu, T. Sasaki, Y. Nakaoka, *J Exp Biol* **2009**, 212, 2767.
- [18] T. Mužič, F. Tounsi, S. B. Madsen, D. Pollakowski, M. Konrad, T. Heimbürg, *Biochim. Biophys. Acta, Biomembr.* **2019**, 1861, 183026.
- [19] T. Parasassi, F. Conti, E. Gratton, *Cell. Mol. Biol.* **1986**, 32, 103.
- [20] T. Parasassi, E. Gratton, *J. Fluoresc.* **1992**, 2, 167.
- [21] T. Parasassi, G. De Stasio, G. Ravagnan, R. M. Rusch, E. Gratton, *Biophys. J.* **1991**, 60, 179.
- [22] S. S. W. Leung, J. Brewer, L. A. Bagatolli, J. L. Thewalt, *Biochim. Biophys. Acta, Biomembr.* **2019**, 1861, 183053.
- [23] C. Stringer, T. Wang, M. Michaelos, M. Pachitariu, *Nat. Methods* **2021**, 18, 100.
- [24] T. Parasassi, E. Gratton, W. M. Yu, P. Wilson, M. Levi, *Biophys. J.* **1997**, 72, 2413.
- [25] L. Weng, F. Ellett, J. Edd, K. H. K. Wong, K. Uygün, D. Irimia, S. L. Stott, M. Toner, *Lab Chip* **2017**, 17, 4077.
- [26] J. B. Fleury, *RSC Adv.* **2020**, 10, 19686.
- [27] M. Burns, K. Wisser, J. Wu, I. Levental, S. L. Veatch, *Biophys. J.* **2017**, 113, 1212.
- [28] M. E. Lalande, V. Ling, R. G. Miller, *Proc. Natl. Acad. Sci. USA.* **1981**, 78, 363.
- [29] B. Snijder, R. Sacher, P. Rämö, E.-M. Damm, P. Liberali, L. Pelkmans, *Nature* **2009**, 461, 520.
- [30] M. Frechin, T. Stoeger, S. Daetwyler, C. Gehin, N. Battich, E.-M. Damm, L. Stergiou, H. Riezman, L. Pelkmans, *Nature* **2015**, 523, 88.
- [31] S. Braig, B. U. Sebastian Schmidt, K. Stoiber, C. Händel, T. Möhn, O. Werz, R. Müller, S. Zahler, A. Koeberle, J. A. Käs, A. M. Vollmar, *New J. Phys.* **2015**, 17, 083007.
- [32] R. S. Vest, L. J. Gonzales, S. A. Permann, E. Spencer, L. D. Hansen, A. M. Judd, J. D. Bell, *Biophys. J.* **2004**, 86, 2251.
- [33] K. Yamamoto, J. Ando, *J. Cell Sci.* **2013**, 126, 1227.
- [34] T. Heimbürg, A. D. Jackson, *Biophys. J.* **2007**, 92, 3159.
- [35] T. Heimbürg, *Biophys. J.* **2012**, 103, 918.
- [36] T. Heimbürg, A. D. Jackson, *Proc. Natl. Acad. Sci. U. S. A.* **2005**, 102, 9790.
- [37] C. Fillafer, A. Paeger, M. F. Schneider, *Prog. Biophys. Mol. Biol.* **2021**, 162, 57.
- [38] S. Preibisch, S. Saalfeld, P. Tomancak, *Bioinformatics* **2009**, 25, 1463.
- [39] D. Liljequist, B. Elfving, K. Skavberg Roaldsen, *PLoS One* **2019**, 14, e0219854.
- [40] T. I. Rokitskaya, G. A. Korshunova, Y. N. Antonenko, *Biophys. J.* **2018**, 115, 514.